View Article Online
View Journal

Green Chemistry

Cutting-edge research for a greener sustainable future

Accepted Manuscript

This article can be cited before page numbers have been issued, to do this please use: C. W. Lim, L. Gao, N. Yan and Y. Xiao, *Green Chem.*, 2024, DOI: 10.1039/D5GC00572H.

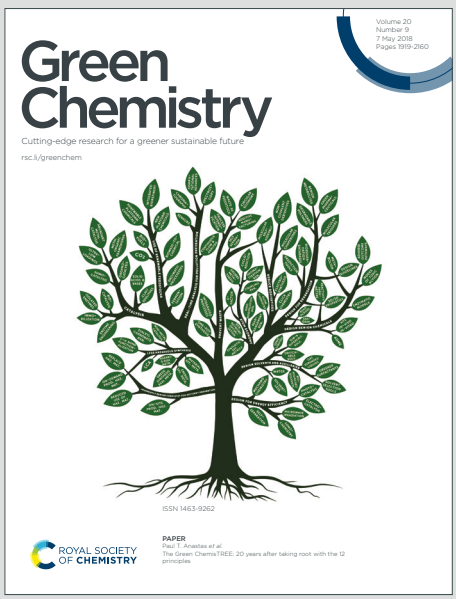

View Article Online
DOI: 10.1039/D5GC00572H

Green Foundation

1. This work presents a benign electrocatalytic strategy for nitrile synthesis from primary alcohols and ammonia. Compared to conventional chemical routes that require toxic reagents, harsh conditions, and generate significant waste, our method eliminates the need for external oxidants and operates under mild conditions.
2. Rather than relying on complex bimetallic catalysts or noble metals like Pd and Au, a simple Ni catalyst is developed. The process enables catalyst reusability without significant loss of performance over multiple cycles.
3. Future research will focus on expanding this method to a broader range of alcohol feedstocks, including biomass-derived alcohols and ammonia from waste streams.

View Article Online
DOI: 10.1039/D5GC00572H

ARTICLE

Electrosynthesis of nitriles from primary alcohols and ammonia on Ni catalyst

Received 00th January 20xx,
Accepted 00th January 20xx

DOI: 10.1039/x0xx00000x

Yiying Xiao,[a,b] Chia Wei Lim,[b] Linfeng Gao [b] and Ning Yan [*a,b]

Despite increasing interest on the electrocatalytic refinery to produce value-added chemicals, heterogeneous nitrile electrosynthesis from alcohols is still in the initial stage of investigation. Here, we report the direct electrosynthesis of nitriles from primary alcohols and ammonia, with a simple nickel catalyst under benign conditions in aqueous electrolytes. The highest benzonitrile Faradaic efficiency of 62.9% and formation rate of 93.2 mmol m^{-2}_{cat} h^{-1} were achieved at room temperature. The reaction proceeds via a dehydrogenation-imination-dehydrogenation sequence, with the rate-determining step likely involving the cleavage of α-carbon C-H bond of the alcohol. Based on the electrochemical and *in-situ* Raman analyses, we propose that the *in-situ* formed Ni^{2+}/Ni^{3+} redox species serves as the active site for converting alcohol to nitrile, while Ni^{2+} also exhibits capability for the oxidation of imine. Various aromatic, aliphatic and heterocyclic primary alcohols were transformed to the corresponding nitriles, exhibiting broad feasibility of our strategy. This study offers a cheap catalyst based electrocatalytic system for the synthesis of high-value nitriles under mild conditions.

Introduction

Due to the increased production of green electricity from renewable energy sources, there has been an increasing interest devoted to the electrocatalytic refinery for the synthesis of value-added chemicals.[1, 2] The benefits afforded by electrocatalytic processes are multi-fold: apart from the fact that electrical energy inputs are readily available from renewable sources, water can be used as a solvent (avoiding the need for organic solvents), and benign operations at or near ambient temperature.[3, 4] In particular, C-N coupling reactions are an important class of reactions for manufacturing various bulk and fine chemicals, such as fertilizers, synthetic fibres, pigments and pharmaceuticals.[5, 6] These reactions involve the formation of carbon-nitrogen bonds between a carbon-based compound and a nitrogen source, giving rise to organonitrogen products. Notable works in electrocatalytic C-N coupling include the electrosynthesis of amines and amides from CO_2 or CO.[7-9] Interestingly, urea has been successfully synthesised from CO_2 and various nitrogenous species.[10, 11] Recently, the valorisation of CO_2-derived formic acid and methanol to formamide has also been demonstrated.[12, 13] Biomass-derived carbonyl compounds are also used for the electrocatalytic reductive amination (ERA) C-N coupling reaction.[14, 15] A special case of ERA uses α-keto acids as the substrate to produce amino acids, which have immense biological uses, utilising various metal and carbon-based cathodes.[16, 17]

Despite the extensive efforts in the wider topic of electrocatalytic C-N coupling, the direct heterogeneous electrosynthesis of nitriles from primary alcohols is not common. Nitriles are versatile intermediates for producing higher value chemicals, including biological materials, pharmaceuticals and polymers.[18, 19] The conventional chemical methods for nitrile synthesis, such as the Sandmeyer[20] and the Rosenmund-von Braun[21] reactions, are not benign as they utilise toxic starting materials, require severe reaction conditions and generate large amounts of chemical waste (Fig. 1a). Improved chemical routes using alcohols and ammonia as the substrates, via ammoxidation[22-28] or oxidant-free dehydrogenation coupled with imination,[29-31] have been recently reported (Supplementary Table S1). However, they face certain issues, including the need for oxidants or high reaction temperatures, as well as poor selectivity due to over-oxidation and other undesired side reactions. On the electrocatalysis front, the synthesis of hydrogen cyanide, an analogue of nitrile, has been demonstrated using methane and ammonia as the substrates,[32] albeit at elevated temperatures of 800-1000 °C with solid electrolytes. The required temperature for hydrogen cyanide synthesis in the solid electrolyte was decreased to 500-650 °C by replacing methane with methanol.[33, 34] In the recent decade, nitriles have been synthesised from alcohols via homogeneous electrocatalysis using 2,2,6,6-tetramethylpiperidinyl-1-oxy (TEMPO) or TEMPO-derived catalysts as mediators, but these methods necessitate additional separation steps for catalyst reuse.[35, 36] Thus far, only limited work has been done for nitrile electrosynthesis from

[a] Joint School of National University of Singapore and Tianjin University, International Campus of Tianjin University, Binhai New City, Fuzhou 350207, China.
[b] Department of Chemical and Biomolecular Engineering, National University of Singapore, 4 Engineering Drive 4, Singapore 117585, Singapore.
Electronic Supplementary Information (ESI) available: DOCX file containing MS spectra, LSV curves, CV curves, HPLC chromatograms, XPS spectra, Raman spectra, *in-situ* Raman setup, NMR spectra, electrochemical measurements, concentration profiles, kinetic modelling, Hammett plot, schemes, tables. See DOI: 10.1039/x0xx00000x

primary alcohols using heterogeneous catalysts. Zhang and co-workers have developed an electro-oxidative coupling strategy for the synthesis of various nitriles with moderate to high selectivities from corresponding alcohols and aqueous ammonia.[37] Their bimetallic electrocatalyst consists of Cu and a noble metal Pd, which acted as the sites for the oxidation and coupling reactions, respectively. More recently, Ma *et al.* designed a NiCo nitride and oxide tandem catalyst for the electrosynthesis of benzonitrile from benzyl alcohol and ammonia.[38] The oxide phase was said to enable the oxidation of alcohol to aldehyde, while the nitride phase allowed for the oxidation of the imine intermediate to the nitrile product. The catalysts in both of these works possess complex structures. Therefore, opportunities exist for electrocatalytic nitrile synthesis from alcohols using cheaper and easily scalable catalysts.

Here, we report a facile one-pot synthesis of various nitriles from primary alcohols and ammonia, in the presence of simple Ni catalyst under ambient temperature using aqueous electrolyte without the need for oxidants (Fig. 1b). Ten materials were first screened and Ni was determined as the optimal catalyst. Several control experiments and kinetic studies were performed to deduce the reaction pathway and rate-limiting step. To understand the metal sites contributing to the catalytic activity, we conducted electrochemical analyses and *in-situ* experiments. The influence of different reaction parameters was also studied.

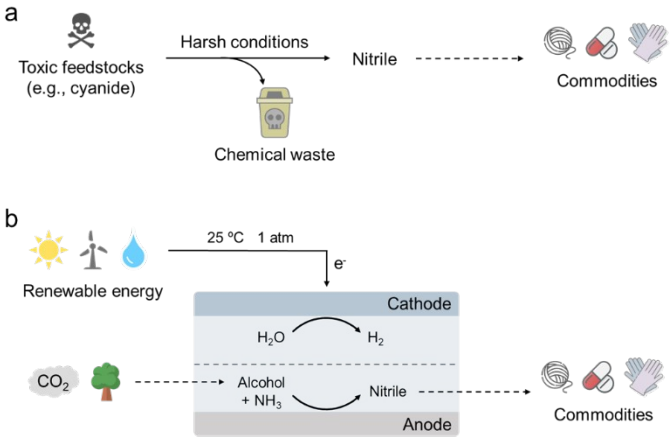

Figure 1. Schematic comparison of the nitrile syntheses. a) Conventional chemical route. **b)** Proposed electrochemical route.

Experimental

Chemicals

Sodium perchlorate ($NaClO_4$, ≥98.0%), sodium hydroxide (NaOH, ≥98.5%), potassium hydroxide (KOH, 90%), ammonia solution (~25 wt. % NH_3 in water), benzyl alcohol (≥99%), benzyl-α,α-d_2 alcohol (99%, D, 98%), benzaldehyde (≥99%), benzoic acid (≥99.5%), benzonitrile (≥99%), benzamide (99%), 4-methylbenzyl alcohol (98%), 4-methylbenzonitrile (98%), 4-methoxybenzyl alcohol (98%), 4-methoxybenzonitrile (99%), 2-hydroxybenzyl alcohol (99%), 2-hydroxybenzonitrile (99%), 4-hydroxybenzyl alcohol (99%), 4-cyanophenol (95%), 4-hydroxy-3-methoxybenzyl alcohol (98%), 4-hydroxy-3-methoxybenzonitrile (98%), 4-chlorobenzyl alcohol (99%), 4-chlorobenzonitrile (99%), 4-nitrobenzyl alcohol (99%), 4-nitrobenzonitrile (97%), 4-nitrobenzamide (98%), furfuryl alcohol (98%), 2-furonitrile (99%), acetamide (~99%), 1-butanol (99.8%), butyronitrile (≥99%), 1-hexanol (≥99%), hexanenitrile (98%), 1,6-hexanediol (99%), adiponitrile (99%), 1-pentanol (≥99%), 3-(trimethylsilyl)-1-propanesulfonic acid sodium salt (97%), hydrochloric acid (HCl, 37%) and sulfuric acid (H_2SO_4, 95.0-98.0%) were purchased from Sigma-Aldrich. Nitric acid (HNO_3, 65%), absolute ethanol (>99.7%) and ethyl acetate (≥99.8%) were provided by VWR Chemicals. Acetone (HPLC grade) and acetonitrile (HPLC grade) were purchased from Fisher Chemical. Deuterium oxide (D_2O, D, 99.9%) and dimethyl sulfoxide-d6 (DMSO-d6, D, 99.9%) was purchased from Cambridge Isotope Laboratories. Nitrogen gas (N_2, 99.9995%) was supplied by Air Liquide. Commercially available reagents were used as received without further purification. All aqueous solutions were prepared using ultra-pure water (Milli-Q®, resistivity of 18.0 MΩ cm).

Preparation of electrodes

Manganese plate (Mn plate, ~1 mm thickness, 99.9%) was purchased from Xingtai Xinnai Metal Materials Co., Ltd. Iron foam (Fe foam, 1.0 mm thickness, 99.9%), cobalt foam (Co foam, 1.6 mm thickness, 99.9%), nickel foam (Ni foam, 1.0 mm thickness, ≥99.9%) and copper foam (Cu foam, 1.0 mm thickness, ≥99.7%) were purchased from Kunshan Guangjiayuan New Materials Co., Ltd. Zinc foam (Zn foam, 1.0 mm thickness, 99.9%) was purchased from Kunshan Lvchuang Electronic Tech Co., Ltd. Ruthenium plate (Ru plate, 1 mm thickness, 99.95%) was purchased from Quanzhou Qijin New Material Tech Co., Ltd. Palladium plate (Pd plate, 0.1 mm thickness, ≥99.98%) was purchased from Wuxi Mini Chemistry Art Meseum Co., Ltd. Platinum plate (Pt plate, 0.1 mm thickness, ≥99.99%) was purchased from Shanghai Chengxin Scientific Instrument Co., Ltd. Carbon paper (CP, TGP-H-060, 0.19 mm thickness) was purchased from Suzhou Sinero Tech Co., Ltd.

Fe, Co, Ni, Cu, Zn and carbon paper electrodes used in this work were cut into 1.5 × 3 cm, while the dimensions of the used-as-received Mn, Ru, Pd and Pt plates were 1 × 1 cm. The cleaning and preparation of metal electrodes were carried out immediately prior to use in every experiment. Fe, Zn and Mn electrodes were mechanically polished using sandpaper, then washed with ultra-pure water. Co, Ni and Cu electrodes were first sonicated with acetone for 30 min before washing with ultra-pure water, then pretreated by immersing in 2 M HCl for 30 min. Ru, Pd and Pt electrodes were stored in 33% HNO_3 until use. The pretreatment of carbon paper was performed through sonicating in 1 M HNO_3 for 30 min. After that, the carbon paper was washed thoroughly using ultra-pure water and absolute ethanol, followed by drying overnight at 80 °C.

View Article Online
DOI: 10.1039/D5GC00579H

Material characterisation

Raman spectra were collected by a Raman microscope (XploRA™ Plus, HORIBA Scientific) with a 638 nm excitation laser using a 100X objective lens. The chemical environments of the Ni foam were identified by X-ray photoelectron spectroscopy (XPS, Kratos AXIS Ultra^{DLD}, Kratos Analytical Ltd.) with mono Al Kα X-ray source. All XPS data were calibrated to C 1s (C-C bond) at 284.50 eV and analysed using XPSPEAK Version 4.1 software. X-ray diffraction (XRD) patterns were obtained by a diffractometer (Bruker D8 Advance), with 2θ ranging from 10° to 80° at a scan rate of 5° min^{-1} and a step size of 0.02°. Scanning electron microscopy (SEM) images were taken on a field emission scanning electron microscope (JEOL JSM-7610F, 5 kV). Inductively coupled plasma-optical emission spectroscopy (ICP-OES) analysis was performed with a Thermo Scientific iCAP 6000 spectrometer.

Electrochemical measurements

All the electrochemical measurements were carried out using a Gamry Interface 1010E potentiostat (Gamry Instruments Inc., U.S.). Similar to our previous study,[16] a glass two-chamber (H-type) three-electrode configurated electrochemical cell, which was separated by a piece of Nafion 117 membrane (N117, Dupont, Xianfeng Instrument Tech Co., Ltd), was used for all experiments. Reference and counter electrodes were a Hg/HgO electrode (1 M KOH) with a double-salt bridge (Shanghai Yueci Electronic Tech Co., Ltd.) and a platinum mesh (Pt mesh, 10 × 10 mm, ≥99.99%, Shanghai Chengxin Scientific Instrument Co., Ltd.), respectively. For H-cell with Fe, Co, Ni, Cu, Zn and carbon paper (4.5 cm^2 area) as working electrodes, the electrolyte volume was 40 mL (50 mL in total volume) for both anodic and cathodic chambers, while for Mn, Ru, Pd and Pt plates (1 cm^2 area) as working electrodes, the electrolyte volume in each chamber was 9 mL (15 mL in total volume). This maintains the same ratio of electrode area to electrolyte volume, ensuring that the conditions were as close as possible for a fair comparison of electrocatalytic performance. In all cases, 15 mL/min purified nitrogen gas was purged through the anodic electrolyte for 30 min at the start of each experiment to exclude the air. During the measurements, the electrolyte solution was stirred and bubbled with nitrogen gas continuously. The potentials applied against the Hg/HgO reference electrode were calibrated to the reversible hydrogen electrode (RHE) scale without iR compensation using the follow equation:

$$E_{\mathrm{RHE}}(\mathrm{V}) = E_{\mathrm{Hg/HgO}}(\mathrm{V}) + 0.098\ \mathrm{V} + 0.059\ \mathrm{V} \times \mathrm{pH} \quad \text{(eq. 1)}$$

All current densities were calculated on the basis of the measured currents and geometric areas of the working electrodes (4.5 cm^2 for Fe, Co, Ni, Cu, Zn foams and carbon paper, 1 cm^2 for Mn, Ru, Pd and Pt plates).

The electrosynthesis of nitriles was performed by chronoamperometry and investigated systematically under different working electrodes, applied potentials, pH, substrate concentrations, ammonia concentrations and substrate types. In a typical electrolysis procedure, certain concentrations of NH_3, $NaClO_4$ and KOH aqueous solution with and without organic substances were used as the anolyte and catholyte, respectively. Specifically, the influence of pH on the catalytic performance was carried out by varying the concentrations of KOH and/or $NaClO_4$ to reach the desired pH values. For example, the electrolyte solution with pH 13 contained 0.1 M $NaClO_4$ and around 0.1 M KOH, prepared by adding the required amount of KOH pellets while monitoring the solution pH with a pH meter. The linear sweep voltammetry (LSV) measurements were performed at a scan rate of 5 mV/s or 10 mV/s under various conditions.

The cyclic voltammetry (CV) measurements were conducted with scan rates ranging from 5 to 200 mV/s under various conditions.

Product identification and quantification

During and after the chronoamperometry test, the electrolyte solution collected from the anodic chamber was immediately analysed by either high-performance liquid chromatography (HPLC), gas chromatography (GC) or ^{1}H nuclear magnetic resonance (NMR) spectroscopy depending on the substrate type. The cathodic electrolyte was also analysed to make sure the membrane was in good condition. Before HPLC and GC analyses, the electrolyte solution was acidified to pH 5−6 by 2 M HCl and filtered through a polyethersulfone (PES) syringe filter (0.22 μm, Microlab Scientific).

The aromatic and heterocyclic compounds were analysed by HPLC (Agilent, 1260 Infinity II), equipped with an InfinityLab Poroshell 120 EC-C18 column (3.0 × 150 mm, 2.7-Micron, 1000 bar) and an ultraviolet-visible (UV) detector (1260 Infinity II Refractive Index detector). 5 mM H_2SO_4 aqueous solution and acetonitrile with 0.2 mL/min flow rate (isocratic elution) were used as the A and B mobile phases, respectively. The column temperature was 30 °C and the injection volume was 3 μL.

The aliphatic substrates (except for ethanol and 1,6-hexanediol) and their derivatives were determined by GC (Agilent, 7890A), equipped with a HP-5 column (30 m × 0.320 mm, 0.25 micron) and a flame ionization detection (FID) detector. Nitrogen was applied as the carrier gas. 1-Pentanol was added in the previously prepared 2 M HCl (used for acidifying the samples) as the internal standard to quantify the substrates, intermediates and products.

The qualitative and quantitative analyses of ethanol, 1,6-hexanediol and their derivatives were carried out by NMR spectroscopy (Bruker Ascend™ 400, 400 MHz) at room temperature with water suppression. In short, 250 μL of the sampled electrolyte solution was mixed with 250 μL of internal standard solution consisting of 3-(trimethylsilyl)-1-propanesulfonic acid sodium salt in D_2O.

The Faradaic efficiency (FE) for target products, side products and intermediates was calculated as follows:

View Article Online
DOI: 10.1039/D5GC00572H

$$\mathrm{FE}(\%) = \frac{n \times C \times V \times F}{Q} \times 100 \quad \text{(eq. 2)}$$

where *n* is the number of electrons required for the formation of the compound (*n* = 2 for aldehyde; *n* = 4 for nitrile, amide and acid), *C* is the molar concentration of the compound, *V* is the volume of the electrolyte, *F* is the Faraday constant (96485 C mol^{-1}), and *Q* represents the total charge passed during the electrolysis.

For the sample preparation for gas chromatography-mass spectroscopy (GC-MS), ^{1}H NMR and ^{13}C NMR analyses, the electrolyte solution (40 mL) from chronoamperometry test was extracted with ethyl acetate (4 × 40 mL) to remove the benzoic acid side product. The organic phase was collected and most of the solvent was evaporated subsequently. GC-MS analysis was carried out on a GC system (Agilent, 7890B) fitted with a HP-5MS column (30 m × 0.250 mm, 0.25 micron) and a mass detector (Agilent, 5977B MSD analyser) using helium as the carrier gas. NMR measurements were conducted with aforementioned spectroscopy (Bruker AscendTM 400, 400 MHz) using DMSO-d6 as the deuterium reagent.

Kinetic modelling of the reaction

A set of time-dependent concentrations of benzyl alcohol, benzaldehyde, benzonitrile and benzoic acid were used to simulate the reaction rate constants. Reaction kinetic parameters were fitted according to the least squares fitting algorithm of MATLAB lsqcurvefit.[39, 40] Several constrains were used to confirm that the fitting curve is reasonable. The kinetic equations and fitting curve are shown in Supplementary Fig. S25.

In-situ Raman spectroscopy measurements

A home-made electrochemical cell shown in Supplementary Fig. S12 was used for *in-situ* Raman spectroscopy experiments. *In-situ* Raman spectra were recorded using the aforementioned Raman microscope (XploRA™ Plus, HORIBA Scientific), with a 638 nm excitation laser and a 10X objective lens, under controlled potentials by the electrochemical workstation (Gamry Interface 1010E potentiostat, Gamry Instruments Inc., U.S.). Further details for the setup and measurements are provided in Supplementary Fig. S12.

Results and Discussion

Ni is the best catalyst among the screened materials

In the initial screening, nine monometallic catalysts which were reported to be active in the thermocatalytic nitrile production from alcohols, including Zn, Mn, Fe, Co, Ni, Cu, Ru, Pd and Pt,[41] as well as carbon paper were studied using benzyl alcohol (BnOH) as a model compound (Fig. 2a). The experiment using Zn was not successful as Zn actively reacted with alkali to release hydrogen. For the other nine materials, Ni delivers benzonitrile (PhCN) as the main product with the highest Faradaic efficiency (FE) of 49.4% and formation rate of 93.2 mmol m^{-2}_{cat} h^{-1}, with the co-generation of benzaldehyde (PhCHO), benzoic acid (PhCOOH) and benzamide ($PhCONH_2$). After extraction by ethyl acetate, the organic phase was analysed using GC-MS, ^{1}H NMR and ^{13}C NMR (Fig. 2b, c, Supplementary Fig. S1), confirming the production of PhCN. Ru also has the capacity for PhCN production, but a significantly lower nitrile FE of 11.2% and an unexpectedly low total FE for the organic products (25.6%) were observed. These are possibly due to the competing ammonia oxidation reaction[42] and dissolution of Ru under oxidative potentials (as indicated by the dark green-coloured electrolyte). In sharp contrast, Mn, Fe, Co, Cu, Pd, Pt, and C show no activity for PhCN production. Among them, Mn, Co and Cu faced severe issues of metal oxidation and leaching under the reaction conditions. We further investigated the electrocatalytic properties of the catalysts using linear sweep voltammetry (LSV), and conducted the electro-oxidation of BnOH without the addition of ammonia. In addition to Ni, Ru, Co and Cu also exhibit activity in converting BnOH to the corresponding oxidative products, with a consumption rate of up to 946.7 mmol m^{-2}_{cat} h^{-1} on Ru (Supplementary Fig. S2). However, the total FEs on Co, Cu and Ru are unsatisfactory, with only 50.3% for Ru and less than 15% for Co and Cu. In the absence of BnOH, Mn, Co, Ni, Cu and Ru exhibit anodic currents before the operating potentials (1.425 V or -0.265 V *vs.* RHE), likely due to metal oxidation (Supplementary Fig. S3a-e). Contrary to Ni and Ru which display LSV current enhancements in the presence of BnOH, Mn, Co and Cu show decreased peak currents, suggesting that the BnOH oxidation rates are very slow on these metals and the metal oxidation is comparatively fast. For Fe, Pd, Pt and C, their LSV curves showed negligible current at 1.425 V *vs.* RHE (Supplementary Fig. S3f-i), implying that these metals are not active towards any reactions, including BnOH oxidation, at this potential. We also conducted electrolysis using these four materials at higher oxidative potentials, but there was still negligible PhCN product formation (Supplementary Table S2). For Mn, Co, and Cu, it may be beneficial to dope another element to stabilise the higher oxidation state metal species, thus reducing the metal dissolution rates.[37, 43, 44]

Nitrile synthesis follows a dehydrogenation-imination-dehydrogenation sequence

In thermocatalysis, there are two possible reaction pathways for nitrile synthesis from primary alcohols and ammonia (Scheme S1).[30] Pathway I starts with the dehydrogenation of alcohol to aldehyde, which then condenses with ammonia to form an imine intermediate. The imine is subsequently dehydrogenated to afford the nitrile product. In pathway II, a direct nucleophilic attack by an ammonia molecule on the α-carbon of the alcohol occurs. This results in an S_N2 substitution of the -OH group with $-NH_2$ group to produce an amine intermediate, which then undergoes sequential dehydrogenations to generate a nitrile product.

A series of control experiments were carried out to determine the main pathway (Table 1). No PhCN was detected in the absence of applied potential, BnOH or ammonia (Entries 1-3),

View Article Online
DOI: 10.1039/D5GC00572H

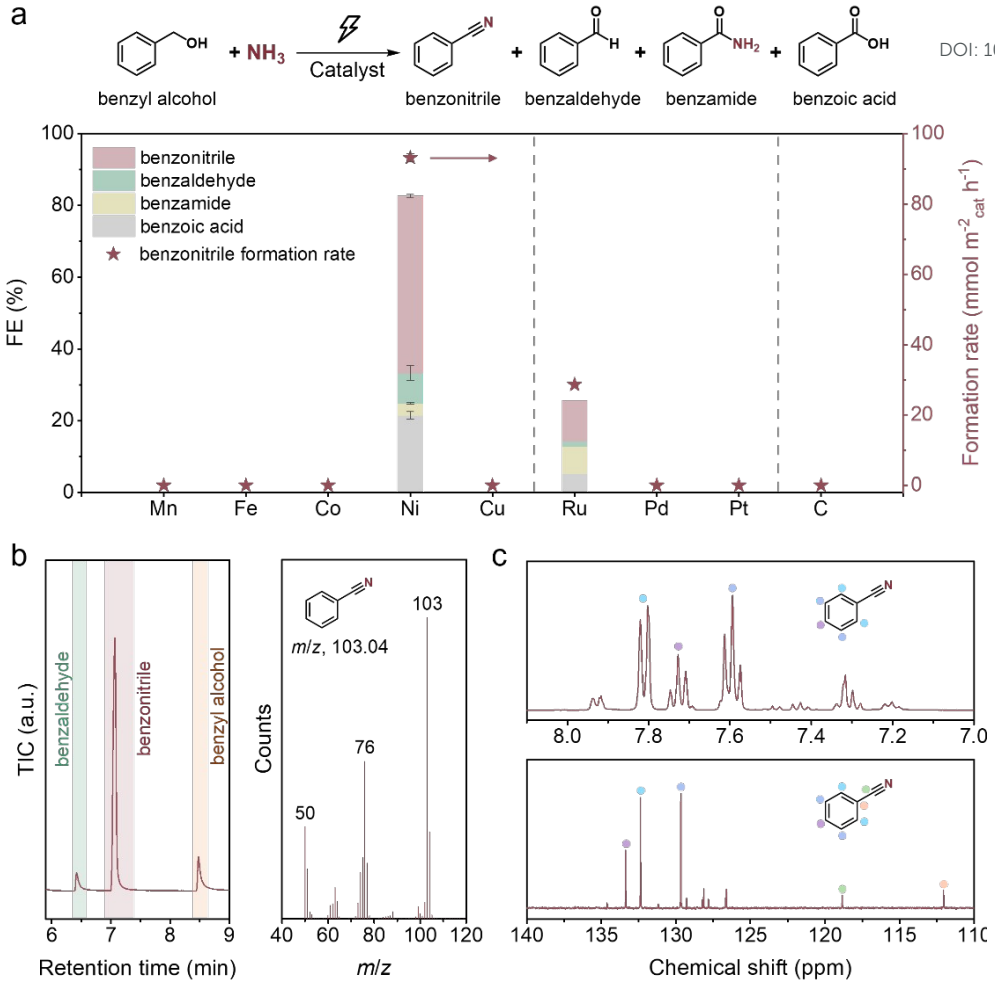

Figure 2. Catalyst screening and performance analysis. a) FEs and PhCN formation rate of electro-oxidative coupling of BnOH and NH_3 on various catalysts. The error bars denote the standard deviation of data from three independent experiments. Reaction conditions: 20 mM BnOH, 1 M NH_3, pH 13, 1.425 V *vs.* RHE (0.675 V *vs.* RHE for Mn), 8 h reaction time (0.5 h for Co and Cu due to significant metal dissolution). Analysis of the extracted liquid carbonaceous compounds obtained from the reaction by **b)** GC-MS (left: GC chromatogram, right: corresponding MS spectrum of PhCN) and **c)** ^{1}H NMR (top) and ^{13}C NMR (bottom). Reaction conditions: Ni foam, 20 mM BnOH, 1 M NH_3, pH 13, 1.425 V *vs.* RHE, 12 h reaction time.

and only the oxidative products of BnOH were generated when ammonia was absent, confirming that PhCN originates from the electro-oxidative coupling of BnOH and ammonia. Notably, when BnOH was replaced by PhCHO, PhCN could be obtained with similar FE of ~50% (Entry 5), demonstrating that PhCHO serves as the key intermediate for nitrile production. We also employed benzylamine ($BnNH_2$) as the carbon source, considering that nitrile could be synthesised from the electrochemical dehydrogenation of amine on Ni-based catalysts.[45-50] Indeed, the electro-oxidation of $BnNH_2$ resulted in PhCN formation, though the FE (74.5%) was rather different from that when using BnOH as the carbon source (Entry 6). Moreover, we were not able to detect $BnNH_2$ intermediate throughout the whole process of BnOH electrolysis (Supplementary Fig. S4, S5a). These results suggest that pathway II via the direct amination of BnOH to yield $BnNH_2$ is highly unlikely.

Table 1. The list of control experiments to confirm the reaction pathway.

Entry	C source	N source	*E* / V *vs.* RHE	Main organic product (FE / %)
1	BnOH	NH_3	×	N.D.
2	×	NH_3	1.425	N.D.
3	BnOH	×	1.425	PhCOOH (94.0)
4	BnOH	NH_3	1.425	PhCN (49.4)
5	PhCHO	NH_3	1.425	PhCN (46.2)
6	$BnNH_2$	NH_3	1.425	PhCN (74.5)
7	PhCN	NH_3	1.425	$PhCONH_2$
8	PhCOOH	NH_3	1.425	N.D.
9	$PhCONH_2$	NH_3	1.425	N.D.

Reaction conditions: Ni foam, 20 mM C source (if present), 1 M N source (if present), pH 13, 1.425 V *vs.* RHE (if present), 8 h reaction time. N.D. = not detected.

To probe the possibility of the various side reactions, PhCN, PhCOOH and $PhCONH_2$ were used to conduct the electrolysis. When PhCN was used as the carbon source, only a trace amount of $PhCONH_2$ was detected, with a $PhCONH_2$ to PhCN ratio of less than 4.5% (Entry 7, Supplementary Fig. S5b, c), which is smaller than the corresponding ratio during BnOH electrolysis (7-8%). This implies that $PhCONH_2$ is probably produced from PhCN hydrolyzation as well as hemiaminal ($PhC(OH)NH_2$) dehydrogenation. Electrolysis using PhCOOH and $PhCONH_2$ failed to generate any organic products (Entries 8, 9). Taken together, the electrocatalytic synthesis of nitrile using primary alcohol and ammonia follows a dehydrogenation-imination-dehydrogenation pathway (Scheme 1). The direct oxidation of aldehyde to form acid serves as the main competing reaction, and the dehydrogenation of hemiaminal intermediate and hydrolyzation of nitrile lead to the amide side product.

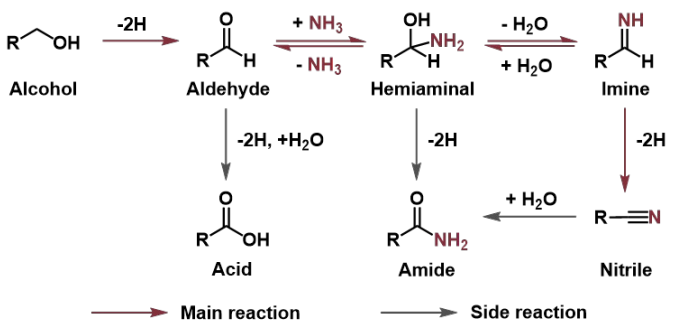

Scheme 1. Plausible reaction pathway in the Ni foam catalysed electro-oxidative coupling of primary alcohols and ammonia to nitriles.

Ni^{2+}/Ni^{3+} redox cycle and Ni^{2+} are active for nitrile synthesis

We initially used LSV to examine the electrochemical properties of Ni foam. In the absence of the organic compounds or ammonia, there is an oxidation peak with an onset at ~1.35 V *vs.* RHE, which is ascribed to the transformation of Ni^{2+} to Ni^{3+} (Fig. 3a, b, eq. 3):

$$Ni(OH)_2 + OH^- \rightleftharpoons NiOOH + H_2O + e^- \quad \text{(eq. 3)}$$

When ammonia is present, the current starts to climb in the same potential region (Supplementary Fig. S6), attributable to the Ni^{3+}-catalysed direct oxidation of ammonia.[51] Upon the addition of BnOH, Ni foam exhibits an oxidative wave with enhanced current density (Fig. 3a), which is also observable in the cyclic voltammetry (CV) curves (Supplementary Fig. S7a). Furthermore, the reduction peak corresponding to the conversion of Ni^{3+} to Ni^{2+} is weakened after introducing BnOH (Supplementary Fig. S7a). A similar phenomenon was observed from the multi-potential chronoamperometry tests, displaying that the reduction current of Ni^{3+} to Ni^{2+} disappeared when BnOH was injected during the open circuit state (Supplementary Fig. S8). We used *ex-situ* X-ray photoelectron spectroscopy (XPS) and Raman spectroscopy to understand this process. As illustrated in the XPS spectra, the surface of the acid-treated Ni foam was mainly composed of metallic Ni and $Ni(OH)_2$ (Supplementary Fig. S9b). When the organic compounds and ammonia were absent, the characteristic peaks associated with Ni^{3+} were detected in both XPS and Raman spectra after applying a potential of 1.45 V *vs.* RHE (Supplementary Fig. S9c, S10). Upon stirring in an electrolyte solution containing BnOH and ammonia, these Ni^{3+} peaks disappeared, while the $Ni(OH)_2$ peak remained and a new peak attributed to NiO appeared (Supplementary Fig. S9d, S10), indicating that $Ni(OH)_2$ and NiO are participating species of the reaction. According to the above results, we deduce that the electrochemically generated Ni^{3+} triggers the C-N coupling of BnOH and ammonia to PhCN, accompanied by the simultaneous reduction of Ni^{3+} to Ni^{2+} (Supplementary Fig. S11, eq. 4a, b), which is likely the widely accepted Ni^{2+}/Ni^{3+}-mediated indirect oxidation of organic compounds:[52]

$$4NiOOH + BnOH + NH_3 \rightarrow 4Ni(OH)_2 + PhCN + H_2O \quad \text{(eq. 4a)}$$
$$4NiOOH + BnOH + NH_3 \rightarrow 4NiO + PhCN + 5H_2O \quad \text{(eq. 4b)}$$

In-situ Raman analyses (Supplementary Fig. S12) were further carried out to verify the assumption through probing the changes in Ni foam during potential alterations. As displayed in Fig. 3c(i), two peaks located at 473 and 553 cm^{-1} are observed above around 1.40 V *vs.* RHE, which correspond to the Ni^{3+}-O bending and stretching vibrations of NiOOH, respectively. The intensities of the NiOOH peaks increase progressively as the potential becomes more positive. The presence of ammonia has insignificant effects on the formation of NiOOH: it only results in slightly decreased peak intensities (Supplementary Fig. S13, S14), possibly due to the partial passivation of the electrode surface by ammonia. When BnOH was added, the NiOOH peaks only accumulate at potentials higher than 1.55 V *vs.* RHE, with distinctly decreased intensities (Fig. 3c(ii)). These results confirm that the *in-situ* formed Ni^{2+}/Ni^{3+} redox species serves as the active site for the PhCN production from BnOH and ammonia, which is consistent with reported computational results showing that the oxidation of alcohol is thermodynamically favourable on NiOOH sites.[53]

Interestingly, compared to that with BnOH and ammonia, the NiOOH peaks start to appear at a negatively shifted potential (~1.45 V *vs.* RHE) with higher intensities when PhCHO intermediate and ammonia are present (Fig. 3(iii)). This is despite a higher current recorded under the *in-situ* Raman measurements (Supplementary Fig. S15), which may imply that the reaction between PhCHO and NiOOH is faster (compared to that between BnOH and NiOOH) and the peaks may be expected to emerge at a more positive potential. Additionally, there is indeed an obvious increase in the Ni^{2+}/Ni^{3+} oxidative current (Fig. 3b, Supplementary Fig. S7b), as well as a decrease in the Ni^{3+}/Ni^{2+} reductive current (Supplementary Fig. S7b) after adding PhCHO. The characteristic peaks attributed to Ni^{3+} were also not discernible after mixing the oxidative-potential-treated Ni foam with PhCHO and ammonia (Supplementary Fig. S9e, S10). Thus, these give us hints that the Ni^{2+}/Ni^{3+} species may be just one of the several possible reactive sites for the C-N coupling of PhCHO and ammonia. Remarkably, given that the onset potential shifts largely in the negative direction to around 1.23 V *vs.* RHE when PhCHO is present (Fig. 3b), it is reasonable

View Article Online
DOI: 10.1039/D5GC00572H

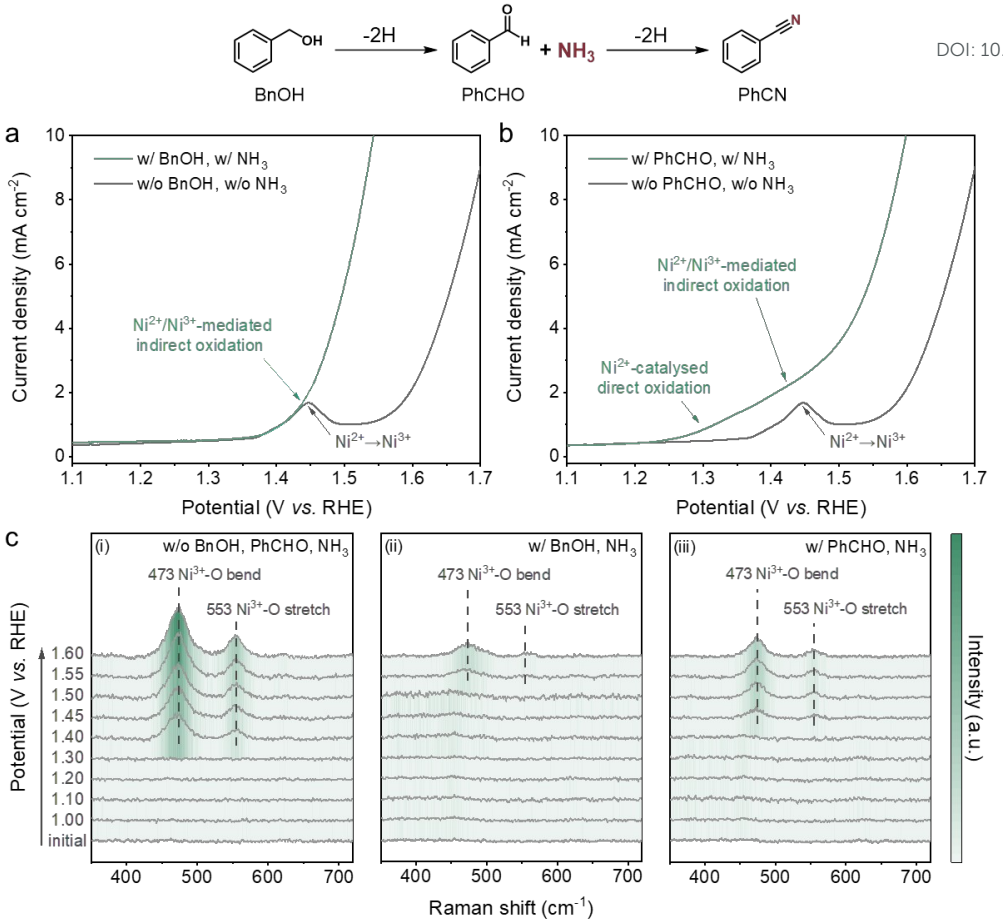

Figure 3. Investigation of the catalytic active sites. a) LSV curves of Ni foam without (grey line) and with (green line) BnOH and NH_3 at a scan rate of 10 mV/s without stirring (pH 13). **b)** LSV curves of Ni foam without (grey line) and with (green line) PhCHO and NH_3 at a scan rate of 10 mV/s without stirring (pH 13). **c)** 2D spectra for the potential-dependent *in-situ* Raman studies of Ni foam **(i)** without BnOH, PhCHO or NH_3; **(ii)** with BnOH and NH_3 and **(iii)** with PhCHO and NH_3. Further details for Raman spectra are given in Supplementary Fig. S14.

to speculate that Ni^{2+} also plays a key role in the oxidative coupling reaction (eq. 5).

$$PhCHO + NH_3 + 2OH^- \xrightarrow{Ni^{2+}} PhCN + 3H_2O + 2e^- \qquad \text{(eq. 5)}$$

To confirm this, we performed electrolysis in the presence of PhCHO and ammonia at 1.27 V *vs.* RHE (Supplementary Fig. S16), where Ni^{3+} does not form (Supplementary Fig. S17, S18). Although at a relatively lower formation rate, PhCN is the only detectable product with a high FE of 74.8%, demonstrating the promising potential of the Ni^{2+} site in the production of nitriles from aldehydes and ammonia. We note that Ni^{2+} has only been hinted, based on LSV studies, as the active site for limited cases of electrochemical oxidative reactions, including cysteine (CySH) dimerisation[54, 55] and N-acetylglucosamine (NAG) oxidation[56] reactions.

Nitrile synthesis depends on potentials, pH and reactant concentrations

The effects of various applied potentials, pH values and ammonia/BnOH concentrations on the FEs and PhCN formation rate of the Ni foam-catalysed electrosynthesis of PhCN were systematically investigated. As the potential becomes more positive than ~1.42 V *vs.* RHE, the PhCN formation rate increases sharply from around 40 to 90 mmol m^{-2}_{cat} h^{-1} and levels off (Fig. 4a), which could be rationalised by earlier LSV results (Fig. 3a). As long as the NiOOH active phase could be rapidly regenerated under these sufficiently positive potentials, the rate of the Ni^{2+}/Ni^{3+}-mediated indirect oxidation of BnOH and ammonia is independent of the applied potentials, which also suggests that the rate-determining step (RDS) directly involves the PhCN formation as opposed to the generation of NiOOH. In the range of 1.35 to 1.50 V *vs.* RHE, the FE towards PhCN firstly increases to its highest value of 62.9% and shows a downward trend at potentials higher than 1.375 V *vs.* RHE.

Notably, the PhCN formation rate exhibits a strong pH dependence, increasing substantially from 0.66 mmol m^{-2}_{cat} h^{-1} (pH 12) to 93.2 mmol m^{-2}_{cat} h^{-1} (pH 13) and declining greatly thereafter (Fig. 4b). The very low PhCN formation rate at pH 12 is likely due to the lack of formation and/or regeneration of NiOOH caused by insufficient OH^- as indicated in eq. 3. Possible reasons for the drops in PhCN formation rate and FE at pH 14 include that (1) the imine formation is suppressed while the geminal diol formation is promoted on account of more prevalent nucleophilic attack by OH^- on imine and aldehyde (Scheme S2);[57] and (2) strong alkaline electrolyte is beneficial for the Cannizzaro reaction and the hydrolysis of nitrile (Scheme

View Article Online
DOI: 10.1039/D5GC00572H

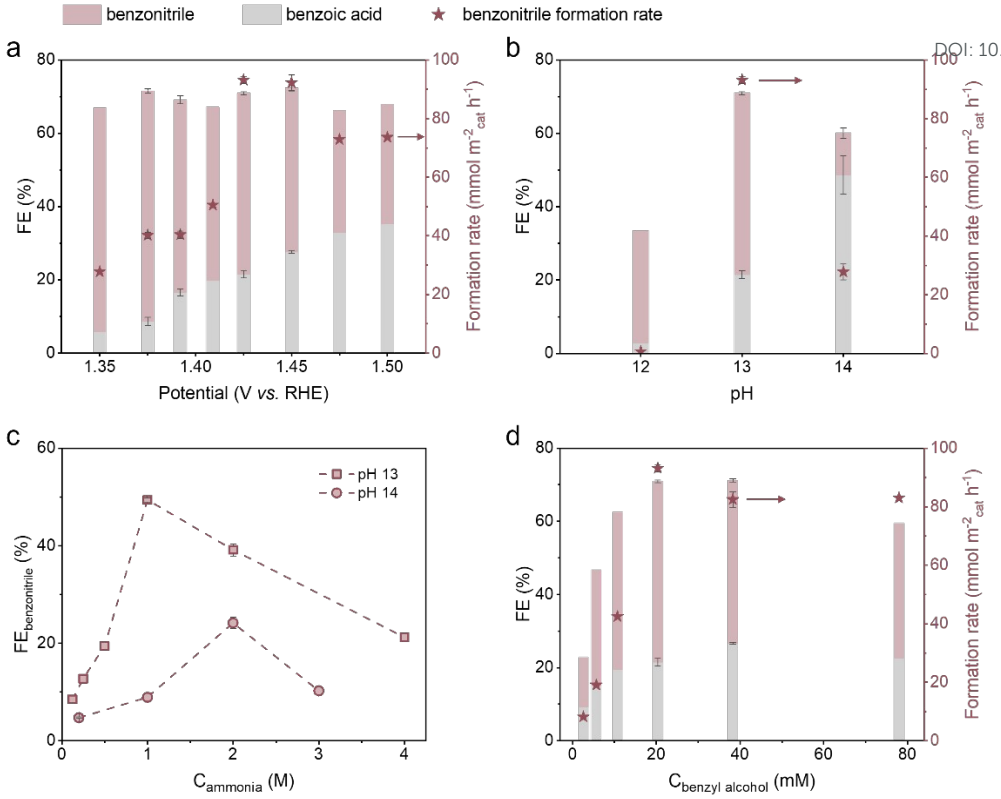

Figure 4. Influence of reaction conditions on PhCN electrosynthesis. FEs and PhCN formation rate of the electro-oxidative coupling of BnOH and NH_3 on Ni foam for 8 h under different **a)** applied potentials (20 mM BnOH, 1 M NH_3, pH 13) and **b)** pH values (20 mM BnOH, 1 M NH_3, 1.425 V *vs.* RHE. **c)** FE of PhCN in the Ni foam catalysed electro-oxidative coupling of BnOH and NH_3 for 8 h under different ammonia concentrations (20 mM BnOH, 1.425 V *vs.* RHE). **d)** FEs and PhCN formation rate of the electro-oxidative coupling of BnOH and NH_3 on Ni foam for 8 h under different BnOH concentrations (1 M NH_3, pH 13, 1.425 V *vs.* RHE). The error bars denote the standard deviation of data from repeated experiments.

S3), leading to the enhancement of acid formation. The lower FE for PhCN at pH 14, in contrast to that at pH 13, is also observed regardless of the ammonia concentrations tested (Fig. 4c). As the ammonia concentration increases, the PhCN FE displays a significant increase, possibly owing to the shifted aldehyde-imine equilibrium to the imine side. There is a decline of FE for PhCN at high ammonia concentrations, probably because ammonia oxidation reaction becomes more favourable. When the BnOH concentration increases, the formation rate and FE of PhCN show remarkable upward trends before being subject to fluctuations (Fig. 4d). The plateau in the PhCN formation rate at BnOH concentrations above 20 mM may be attributed to the saturation of the Ni^{3+} sites, whose rate of transformation from Ni^{2+} now limits the overall rate of PhCN formation.

Overall, we attained a high PhCN FE (62.9%) and selectivity (59.8%) at a relatively low NH_3 concentration (1 M) and overpotential (1.375 V *vs.* RHE) using a simple monometallic electrocatalyst, unlike existing reports which require at least two distinct phases in their catalysts to achieve comparable selectivity (Supplementary Fig. S19). We further performed recycling test over the Ni electrode, which shows that the FE and yield of PhCN were stable over six cycles (Supplementary Fig. S20), demonstrating the good durability of our Ni foam catalyst. A very small amount of Ni dissolution was induced (less than 1‰ of the Ni foam, by mass) during the electrolysis, as quantified by inductively coupled plasma-optical emission spectroscopy (ICP-OES) (Supplementary Table S3). The scanning electron microscopy (SEM) images and X-ray diffraction (XRD) patterns indicate that there are no obvious changes of the morphology and crystal phase of the spent Ni catalyst compared with its original stage (Supplementary Fig. S21, S22).

The rate-determining step involves the alcohol α-carbon C-H bond cleavage

Kinetic analyses were carried out to further understand the RDS of the reaction at pH 13 and 1.425 V *vs.* RHE. The formation of PhCN was first order with respect to BnOH at low concentrations, attaining an approximately zeroth-order dependence at BnOH concentrations beyond 20 mM. (Fig. 5a). Similarly, a roughly first-order dependence on ammonia concentration was determined at lower concentrations, whereas a negative order was obtained above 1 M NH_3 (Fig. 5b). The negative order could be rationalised by the ammonia poisoning effect, which is also revealed in the correlation between BnOH consumption rate and ammonia concentration (Supplementary Fig. S23).

On the basis of the proposed reaction pathway (Scheme 1) and observed reaction orders, we conducted kinetic modelling of the reaction (Supplementary Fig. S25) to fit the experimental results as depicted in Supplementary Fig. S5a. Due to the limited

View Article Online
DOI 10.1039/D5GC00572H

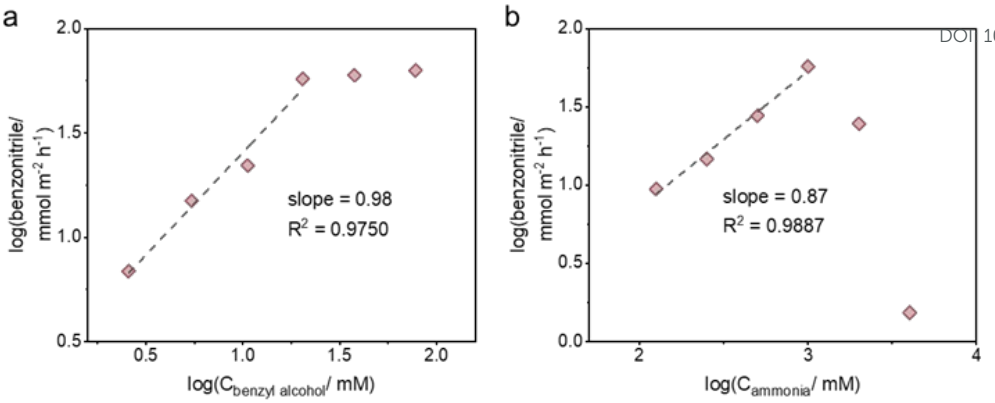

Figure 5. Kinetic measurements of PhCN electrosynthesis. The dependences of PhCN formation rate on the concentration of **a)** BnOH (1 M NH_3) and **b)** NH_3 (20 mM BnOH) at pH 13, 1.425 V *vs.* RHE and conversion around 20%.

concentration of the $PhCONH_2$ side product throughout the period of reaction (< 3% yield), a simplified reaction scheme (Scheme 2) was used. We also performed an experiment to verify that the equilibrium between PhCHO and NH_3 is established instantaneously (Supplementary Fig. S24). The kinetic model predictions agree reasonably well with the experimental results and the optimised parameters are displayed in Table 2, where k_1, k_2 and k_3 refer to the rate constants for the production of PhCHO, PhCN and PhCOOH, respectively, while K is the equilibrium constant for the reversible reaction between PhCHO and imine. The fact that k_1 has the lowest value implies that the RDS may involve the dehydrogenation of BnOH to form PhCHO. We note that our deduction is different from previous work demonstrating that the RDS is the coupling of surface-adsorbed PhCHO* and NH_2* as the C-N coupling was said to occur at the Pd/CuO heterojunction in their system.[37] On the contrary, our catalyst is monometallic, and a slow C-N coupling step occurring on our catalyst is very unlikely. Furthermore, the direct nucleophilic attack by free NH_3 on PhCHO (adsorbed or free) is likely to be much faster than a surface C-N coupling.[13] Thus, it is highly improbable that the RDS involves C-N coupling in our reaction.

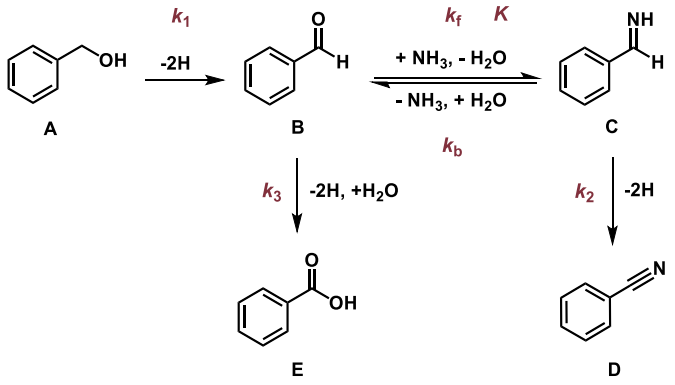

Scheme 2. Simplified reaction pathway used for the modelling of the Ni foam catalysed benzonitrile synthesis from benzyl alcohol and ammonia.

Table 2. Kinetic modelling of the reaction rate constants (k_i) and equilibrium constant (K).

k_1 / h^{-1}	k_2 / h^{-1}	k_3 / h^{-1}	K / mM^{-1}
0.211	2.77	0.13	1.02×10^{-4}

Reaction conditions: Ni foam, 20 mM BnOH, 1 M NH_3, pH 13, 1.425 V *vs.* RHE.

A kinetic isotope effect (KIE) study was performed to determine whether the RDS is the C-H bond cleavage at the α-carbon or the O-H bond breakage in the hydroxyl group of BnOH. The undeuterated substrate ($PhCH_2OH$) and $PhCD_2OH$ (deuteration of both α-hydrogen of benzyl alcohol) were transformed to PhCN under the same reaction conditions. As exhibited in Table 3, the formation rate of $PhCD_2OH$ is smaller than that of $PhCH_2OH$, yielding a KIE value of 1.73. The observed normal KIE value suggests that the α-hydrogen abstraction through a hydrogen atom transfer mechanism may indeed be the RDS for the overall reaction (eq. 6).

$$(PhCH_2OH)_{ads} + NiOOH \xrightarrow{RDS} (Ph\dot{C}HOH)_{ads} + Ni(OH)_2 \quad \text{(eq. 6)}$$

It is worth mentioning that Choi *et al.* have demonstrated another novel mechanism involving hydride transfer from α-hydrogen in alcohols to Ni^{4+} site in NiOOH.[58, 59] Considering that this mechanism happens at more positive potentials (> 1.5 V *vs.* RHE) and is potential-dependent with the regeneration of the catalytically active species as the RDS, we rule out the possibility of this pathway in our case.

Table 3. Kinetic isotopic effects for PhCN electrosynthesis.

Entry	Alcohol	PhCN formation rate / mmol m^{-2}_{cat} h^{-1}	KIE
1	$PhCH_2OH$	57.3	
2	$PhCD_2OH$	33.2	
3	$k_{PhCH_2OH}/k_{PhCD_2OH}$		1.73

Reaction conditions: Ni foam, 20 mM $PhCH_2OH$ or $PhCD_2OH$, 1 M NH_3, pH 13, 1.425 V *vs.* RHE, around 20% conversion.

View Article Online
DOI: 10.1039/D5GC00572H

Electrosynthesis on Ni extends to other nitriles

A series of aromatic, aliphatic and heterocyclic primary alcohols were used as substrates to study the performance of our electrocatalytic system at synthesising the corresponding nitriles. Initially, we used aromatic substrates with electron-donating and withdrawing groups at the para- or ortho-position, which showed moderate to high performances (Fig. 6). A few substrates with electron-donating groups delivered very low to negligible conversions (Supplementary Table S4). Based on literature[60, 61] and our LSV analysis (Supplementary Fig. S26), a probable reason for the inactivity is the passivation of the Ni foam brought about by a radical polymerisation process, as the substituents may be converted to negatively charged phenoxide ions under alkaline reaction conditions. Among the aromatic substrates para-substituted with electron-withdrawing groups (-Cl and -NO_2), the conversions are relatively high (above 87%), although the nitrile selectivities are lower than that obtained using BnOH as the substrate (Fig. 6). This is mainly due to much higher amide selectivities (compared to that of using BnOH as substrate) on these substituted substrates (Supplementary Table S5). Similar phenomena of depressed nitrile selectivity and high amide selectivity were seen when using furfuryl alcohol as the substrate. Interestingly, the 2-furonitrile (**2i**) was observed to convert rapidly and completely to the amide on standing, within a relatively short period even without stirring. Remarkably, the Hammet plot (Supplementary Fig. S27) exhibits a good linear correlation with a positive slope,[62] implying that the rate-determining alcohol dehydrogenation step involves more proton-transfer than electron-transfer character.[63, 64] Meanwhile, the aliphatic alcohols could also be transformed to corresponding nitriles, albeit with lower selectivities. As a majority of these substrates have been reported to be derivable from lignocellulose and/or CO_2,[65-69] our electrosynthetic strategy shows promising feasibility at valorising renewable feedstocks and/or waste materials to make organonitrogen products.

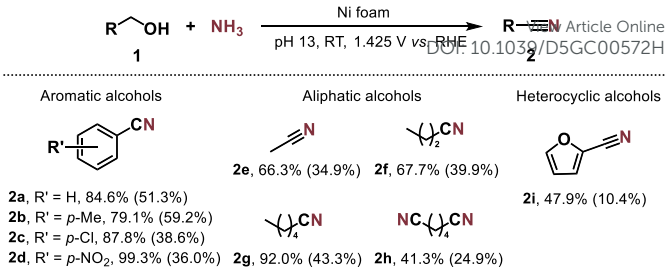

Figure 6. Substrate scope of the electrosynthesis of nitriles from primary alcohols and ammonia. Reaction conditions: Ni foam, 20 mM primary alcohol (5 mM for **1b**, **1c** and **1d**), 1 M NH_3, pH 13, 1.425 V *vs.* RHE, 8 h reaction time. Conversions and selectivities are indicated below each compound, with the latter in parentheses.

Electrosynthesis of nitrile is enhanced at higher temperature

In principle, the reaction pathways leading to different products have different activation energies, thus varying the reaction temperature may alter the product distribution. We conducted the PhCN electrosynthesis from BnOH and NH_3 on Ni catalyst at temperatures between 0 and 60 °C and regulated the applied potential at 50 °C (Supplementary Fig. S28). The LSV curves of the electrocatalytic system were obtained at a range of temperatures (Supplementary Fig. S29), and the potential that gave the same current density as 1.45 V *vs.* RHE at 30 °C was identified for use at each non-room temperature point. Notably, both the yield and FE of PhCN increased sharply as temperature increased from 0 to 50 °C, indicating that the PhCN synthesis is favoured at higher temperatures (Fig. 7a). On the contrary, as the temperature increased to 60 °C, PhCN yield dipped slightly while the total FEs of the organic products decreased significantly, implying that a sizeable portion of the current is attributable to nickel oxidation. As 50 °C is the optimal temperature for PhCN production, we conducted further optimisation at this temperature, where several potentials were found to give PhCN yields exceeding 50% after 3 h (Fig. 7b). The highest PhCN yield of 61.1% was achieved using 20mM BnOH and 1 M NH_3 under an applied potential of 1.392 V *vs.* RHE at 50 °C after 5 h. The studied conditions at 50 °C that resulted in PhCN yields larger than 50% are summarised in Table 4.

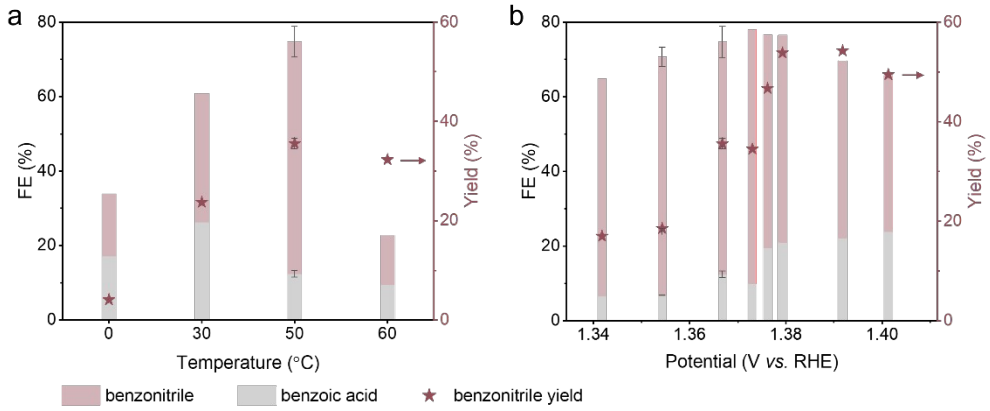

Figure 7. PhCN electrosynthesis over a range of temperature. FEs and PhCN yield of the electro-oxidative coupling of BnOH and NH_3 on Ni foam for 3 h under different **a)** temperatures (20 mM BnOH, 1 M NH_3, pH 13, the applied potentials were chosen based on LSV curves in Supplementary Fig. S29) and **b)** potentials (20 mM BnOH, 1 M NH_3, pH 13, 50 °C). The error bars denote the standard deviation of data from two independent experiments.

Compared to existing thermal catalytic pathways, our system operates at more benign conditions, and the catalysts are based on cheap metal with simple structure (comparison provided in Supplementary Table S1). Relative to the demonstrated electrocatalytic approaches, our system provides comparable or better performance, in terms of the nitrile yield and FE, while requiring a lower NH_3 concentration, oxidative potential, similar or shorter reaction durations and simpler monometallic non-noble metal catalyst (Supplementary Table S6).

Table 4. Electrosynthesis of PhCN from BnOH and NH_3 on Ni catalyst at 50 °C.

Entry	Potential / V *vs.* RHE	Duration / h	PhCN Yield / %	PhCN Selectivity / %
1	1.367	8	54.1	65.8
2	1.376	6	55.8	65.1
3	1.379	6	59.9	67.9
4	1.392	5	61.1	62.6

Reaction conditions: Ni foam, 20 mM BnOH, 1 M NH_3, pH 13, 50 °C.

Conclusions

We have utilised Ni foam for the electrocatalytic synthesis of benzonitrile from benzyl alcohol, with the highest formation rate of 93.2 mmol m^{-2}_{cat} h^{-1} and FE of 62.9%. The reaction likely follows a dehydrogenation-imination-dehydrogenation pathway, with the oxidation of the aldehyde intermediate to carboxylic acid being the main competing reaction and amide as another side product. Ni^{2+}/Ni^{3+} redox species acts as a key site for the C-N coupling between benzyl alcohol and ammonia to produce benzonitrile. The kinetic studies revealed that the extraction of the α-hydrogen from the primary alcohol via a hydrogen atom transfer mechanism is likely the overall rate-limiting step. Notably, we showed that Ni^{2+} is a plausible site for the oxidative coupling, specifically for the oxidation of imine to nitrile, which has not been reported so far. In all, we have demonstrated a noble-metal-free monometallic catalyst for the electrocatalytic nitrile synthesis from primary alcohols. Given the established electrocatalytic pathways from nitrogen-containing ions present in wastewater (NO_3^-, NO_2^-) to NH_3, our work is potentially an enabler of the environmentally sustainable electrosynthesis of valuable nitrile compounds purely using waste materials (CO_2, waste biomass, wastewater) as feedstocks.

Author contributions

N.Y.: Conceptualization, Methodology, Formal Analysis, Resources, Writing – Review & Editing, Supervision, Funding Acquisition. **Y.X.:** Conceptualization, Methodology, Formal Analysis, Investigation, Writing – Original Draft, Writing – Review & Editing, Visualization. **C.W.L.:** Formal Analysis, Investigation, Writing – Original Draft, Writing – Review & Editing. **L.G.:** Methodology, Formal Analysis, Writing – Review & Editing.

Conflicts of interest

View Article Online
DOI: 10.1039/D5GC00572H

There are no conflicts to declare.

Data availability

The data supporting this article have been included as part of the ESI.

Acknowledgements

We thank the National Research Foundation Singapore NRF Investigatorship (Award No. NRF-NRFI07–2021–0006) for supporting this work. We appreciate Dr. Zeliang Yuan for performing XPS measurements. We express our gratitude to Professor Kang Zhou for helping with the fabrication of *in-situ* Raman electrochemical cell. We thank Dr. Hua An for assisting in the temperature-controlled experiments.

References

1 J. G. J. Olivier, J. A. H. W. Peters and G. Janssens-Maenhout, *Trends in global CO_2 emissions. 2012 Report*, Netherlands, 2012.
2 C. Tang, Y. Zheng, M. Jaroniec and S.-Z. Qiao, *Angew. Chem. Int. Ed.*, 2021, **60**, 19572-19590.
3 D. Bogdanov, M. Ram, A. Aghahosseini, A. Gulagi, A. S. Oyewo, M. Child, U. Caldera, K. Sadovskaia, J. Farfan, L. De Souza Noel Simas Barbosa, M. Fasihi, S. Khalili, T. Traber and C. Breyer, *Energy*, 2021, **227**, 120467.
4 S. Chu, Y. Cui and N. Liu, *Nat. Mater.*, 2017, **16**, 16-22.
5 J. Li, Y. Zhang, K. Kuruvinashetti and N. Kornienko, *Nat. Rev. Chem.*, 2022, **6**, 303-319.
6 N. Kurig and R. Palkovits, *Green Chem.*, 2023, **25**, 7508-7517.
7 Y. Wu, Z. Jiang, Z. Lin, Y. Liang and H. Wang, *Nat. Sustain.*, 2021, **4**, 725-730.
8 M. Jouny, J.-J. Lv, T. Cheng, B. H. Ko, J.-J. Zhu, W. A. Goddard and F. Jiao, *Nat. Chem.*, 2019, **11**, 846-851.
9 J. Li and N. Kornienko, *Chem. Sci.*, 2022, **13**, 3957-3964.
10 Y. Wang, D. Chen, C. Chen and S. Wang, *Acc. Chem. Res.*, 2024, **57**, 247-256.
11 C. Yang, Z. Li, J. Xu, Y. Jiang and W. Zhu, *Green Chem.*, 2024, **26**, 4908-4933.
12 C. Guo, W. Zhou, X. Lan, Y. Wang, T. Li, S. Han, Y. Yu and B. Zhang, *J. Am. Chem. Soc.*, 2022, **144**, 16006-16011.
13 N. Meng, J. Shao, H. Li, Y. Wang, X. Fu, C. Liu, Y. Yu and B. Zhang, *Nat. Commun.*, 2022, **13**, 5452.
14 J. J. Roylance and K.-S. Choi, *Green Chem.*, 2016, **18**, 5412-5417.
15 S. D. Mürtz, N. Kurig, F. J. Holzhäuser and R. Palkovits, *Green Chem.*, 2021, **23**, 8428-8433.
16 Y. Xiao, C. W. Lim, J. Chang, Q. Yuan, L. Wang and N. Yan, *Green Chem.*, 2023, **25**, 3117-3126.
17 M. Li, Y. Wu, B.-H. Zhao, C. Cheng, J. Zhao, C. Liu and B. Zhang, *Nat. Catal.*, 2023, **6**, 906-915.
18 M. J. Hülsey, H. Yang and N. Yan, *ACS Sustain. Chem. Eng.*, 2018, **6**, 5694-5707.
19 X. Chen, S. Song, H. Li, G. Gözaydın and N. Yan, *Acc. Chem. Res.*, 2021, **54**, 1711-1722.
20 C. Galli, *Chem. Rev.*, 1988, **88**, 765-792.
21 J. Lindley, *Tetrahedron*, 1984, **40**, 1433-1456.
22 T. Senthamarai, V. G. Chandrashekhar, N. Rockstroh, J. Rabeah, S. Bartling, R. V. Jagadeesh and M. Beller, *Chem*, 2022, **8**, 508-531.

23 H. Wang, D. Xu, E. Guan, L. Wang, J. Zhang, C. Wang, S. Wang, H. Xu, X. Meng, B. Yang, B. C. Gates and F.-S. Xiao, *ACS Catal.*, 2020, **10**, 6299-6308.
24 T. Oishi, K. Yamaguchi and N. Mizuno, *Angew. Chem. Int. Ed.*, 2009, **48**, 6286-6288.
25 W. Yin, C. Wang and Y. Huang, *Org. Lett.*, 2013, **15**, 1850-1853.
26 R. V. Jagadeesh, H. Junge and M. Beller, *Nat. Commun.*, 2014, **5**, 4123.
27 S. Shang, L. Wang, W. Dai, B. Chen, Y. Lv and S. Gao, *Catal. Sci. Technol.*, 2016, **6**, 5746-5753.
28 J. He, P. Zhou, S. Zhang, J. C.-H. Lam, Y. Liao and Z. Zhang, *Green Chem.*, 2024, **26**, 1831-1845.
29 Y. Hu, S. Jin, Z. Zhang, L. Zhang, J. Deng and H. Zhang, *Catal. Commun.*, 2014, **54**, 45-49.
30 Y. Wang, S. Furukawa, Z. Zhang, L. Torrente-Murciano, S. A. Khan and N. Yan, *Catal. Sci. Technol.*, 2019, **9**, 86-96.
31 Y. Wang, S. Furukawa and N. Yan, *ACS Catal.*, 2019, **9**, 6681-6691.
32 N. Kiratzis and M. Stoukides, *J. Electrochem. Soc.*, 1987, **134**, 1925-1929.
33 N. Kiratzis and M. Stoukides, *J. Catal.*, 1991, **132**, 257-262.
34 A. Raj, R. A. Rudkin and A. Atkinson, *J. Electrochem. Soc.*, 2010, **157**, B719.
35 Z. Fan, X. Yang, C. Chen, Z. Shen and M. Li, *J. Electrochem. Soc.*, 2017, **164**, G54.
36 R. M. Rodrigues, D. A. Thadathil, K. Ponmudi, A. George and A. Varghese, *ChemistrySelect*, 2022, **7**, e202200081.
37 Z. Fang, Y. Ding, M. Wang, L. Wang, F. Li, K. Fan, X. Wu, L. Sun and P. Zhang, *Appl. Catal. B*, 2023, **337**, 122999.
38 T. Mushiana, Z. Shao, M. Khan, N. Zhang and M. Ma, *Chem. Eng. J.*, 2023, **477**, 146742.
39 S. Siankevich, G. Savoglidis, Z. Fei, G. Laurenczy, D. T. L. Alexander, N. Yan and P. J. Dyson, *J. Catal.*, 2014, **315**, 67-74.
40 S. Song, Y. Wang and N. Yan, *Mol. Catal.*, 2018, **454**, 87-93.
41 Y. Wang, S. Furukawa, X. Fu and N. Yan, *ACS Catal.*, 2020, **10**, 311-335.
42 N. M. Adli, H. Zhang, S. Mukherjee and G. Wu, *J. Electrochem. Soc.*, 2018, **165**, J3130.
43 J. Zhu, J. Shao, B.-A. Shen, J. Chen, Y. Yu, S. Song, X.-B. Zhang, B. Zhang and B.-H. Zhao, *JACS Au*, 2023, **3**, 2987-2992.
44 Y. Tang, X. Li, H. Lv, D. Xie, W. Wang, C. Zhi and H. Li, *Adv. Energy Mater.*, 2020, **10**, 2000892.
45 P. M. Robertson, *J. Electroanal. Chem. Interf. Electrochem.*, 1980, **111**, 97-104.
46 Y. Huang, X. Chong, C. Liu, Y. Liang and B. Zhang, *Angew. Chem. Int. Ed.*, 2018, **57**, 13163-13166.
47 W. Wang, Y. Wang, R. Yang, Q. Wen, Y. Liu, Z. Jiang, H. Li and T. Zhai, *Angew. Chem. Int. Ed.*, 2020, **59**, 16974-16981.
48 W. Chen, C. Xie, Y. Wang, Y. Zou, C.-L. Dong, Y.-C. Huang, Z. Xiao, Z. Wei, S. Du, C. Chen, B. Zhou, J. Ma and S. Wang, *Chem*, 2020, **6**, 2974-2993.
49 M. T. Bender and K.-S. Choi, *JACS Au*, 2022, **2**, 1169-1180.
50 Y. Sun, H. Shin, F. Wang, B. Tian, C.-W. Chiang, S. Liu, X. Li, Y. Wang, L. Tang, W. A. Goddard, III and M. Ding, *J. Am. Chem. Soc.*, 2022, **144**, 15185-15192.
51 A. Kapałka, A. Cally, S. Neodo, C. Comninellis, M. Wächter and K. M. Udert, *Electrochem. Commun.*, 2010, **12**, 18-21.
52 M. Fleischmann, K. Korinek and D. Pletcher, *J. Electroanal. Chem. Interf. Electrochem.*, 1971, **31**, 39-49.
53 L. Wei, M. D. Hossain, M. J. Boyd, J. Aviles-Acosta, M. E. Kreider, A. C. Nielander, M. B. Stevens, T. F. Jaramillo, M. Bajdich and C. Hahn, *ACS Catal.*, 2023, **13**, 4272-4282.
54 D. Giovanelli, N. S. Lawrence, L. Jiang, T. G. J. Jones and R. G. Compton, *Sens. Actuators B Chem.*, 2003, **88**, 320-328.
55 D. Jia, F. Li, L. Sheng, Q. Ren, S. Dong, S. Xu, Y. Mu and Y. Miao, *Electrochem. Commun.*, 2011, **13**, 1119-1122.
56 H. Zhao, D. Lu, J. Wang, W. Tu, D. Wu, S. W. Koh, P. Gao, Z. J. Xu, S. Deng, Y. Zhou, B. You and H. Li, *Nat. Commun.*, 2021, **12**, 2008.
57 H. J. Schäfer, *Electrochemistry I*, 1987.
58 M. T. Bender, Y. C. Lam, S. Hammes-Schiffer and K.-S. Choi, *J. Am. Chem. Soc.*, 2020, **142**, 21538-21547.
59 M. T. Bender, R. E. Warburton, S. Hammes-Schiffer and K.-S. Choi, *ACS Catal.*, 2021, **11**, 15110-15124.
60 P. Parpot, A. P. Bettencourt, A. M. Carvalho and E. M. Belgsir, *J. Appl. Electrochem.*, 2000, **30**, 727-731.
61 C. Z. Smith, J. H. P. Utley and J. K. Hammond, *J. Appl. Electrochem.*, 2011, **41**, 363-375.
62 C. Hansch, A. Leo and R. W. Taft, *Chem. Rev.*, 1991, **91**, 165-195.
63 D. R. Weinberg, C. J. Gagliardi, J. F. Hull, C. F. Murphy, C. A. Kent, B. C. Westlake, A. Paul, D. H. Ess, D. G. McCafferty and T. J. Meyer, *Chem. Rev.*, 2012, **112**, 4016-4093.
64 M. J. Chalkley, P. Garrido-Barros and J. C. Peters, *Science*, 2020, **369**, 850-854.
65 J. Xu, J. Meng, Y. Hu, Y. Liu, Y. Lou, W. Bai, S. Dou, H. Yu and S. Wang, *Research*, 2023, **6**, 0288.
66 F. Li, Y. C. Li, Z. Wang, J. Li, D.-H. Nam, Y. Lum, M. Luo, X. Wang, A. Ozden, S.-F. Hung, B. Chen, Y. Wang, J. Wicks, Y. Xu, Y. Li, C. M. Gabardo, C.-T. Dinh, Y. Wang, T.-T. Zhuang, D. Sinton and E. H. Sargent, *Nat. Catal.*, 2020, **3**, 75-82.
67 I. Lauer, G. Philipps and S. Jennewein, *Microb. Cell Fact.*, 2022, **21**, 85.
68 J. He, S. P. Burt, M. Ball, D. Zhao, I. Hermans, J. A. Dumesic and G. W. Huber, *ACS Catal.*, 2018, **8**, 1427-1439.
69 Y. Jing, Y. Guo, Q. Xia, X. Liu and Y. Wang, *Chem*, 2019, **5**, 2520-2546.

The data supporting this article have been included as part of the ESI. Original data is available from the authors upon reasonable request.

View Article Online
DOI: 10.1039/D5GC00572H